Inorganic Chemistry

Article

pubs.acs.org/IC

Ruthenium(II) Thiacrown Complexes Incorporating Noninnocent Redox Active Ligands: Synthesis, Electrochemical Properties, and Theoretical Studies

James D. Ingram,[†] Paulo J. Costa,[‡] Harry Adams,[†] Michael D. Ward,*[,†] Vítor Félix,*[,‡] and Jim A. Thomas*[,†]

[†]Department of Chemistry, University of Sheffield, Sheffield S3 7HF, U.K.

[‡]Departamento de Química, CICECO and Secção Autónoma de Ciências da Saúde, Universidade de Aveiro, 3810-193, Aveiro, Portugal

Supporting Information

ABSTRACT: The synthesis and characterization of a series of nine new complexes incorporating $[Ru^{II}Cl([n]aneS_3)]$ (n = 12,14, 16) metal centers coordinated to redox active catechol ligands is reported. The solid-state structure of one of these complexes has been determined by X-ray crystallography. The redox properties of these complexes have been probed experimentally through absorption spectroscopy, cyclic voltammetry, and spectroelectrochemistry, as well as computationally through density functional theory calculations. These studies reveal that, whereas the tetrachlorocatechol-based complexes are isolated with the dioxolene unit in the catechol form, the rest of the complexes are isolated in the semiquinone oxidation state. It was also found that the $Ru^{III/II}$-based couple for the complexes is dependent on the nature of the thiacrown ligand coordinated to the metal center. A combination of optical and theoretical studies revealed that the absorption spectra of the complexes contain contributions from a variety of charge transfer processes; in the case of the tetrachlorocatechol complexes these transitions include catechol-to-thiacrown ligand-to-ligand charge transfer.

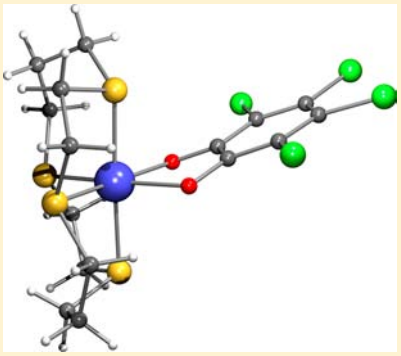

INTRODUCTION

In metal complexes, noninnocent redox behavior occurs when the oxidation states of the metal and a coordinated ligand cannot be defined without ambiguity.[1] Noninnocence arises when the frontier orbitals of the metal and the ligand are close enough in energy for mixing to occur, and is therefore dependent on both the ligand and the metal. This phenomenon has been observed in the active site of metallo-enzymes[2] and is also exploited in the construction of novel redox-active catalysts.[3] Although this phenomenon was first studied in detail in dithiolene complexes,[1,4] transition metal complexes of another redox active ligand, catechol, have also attracted much interest.[5−15]

The redox properties of catechol (1,2-dihydroxybenzene) are well-known: deprotonation of both hydroxy groups yields a dianion, which can then be oxidized by two electrons to o-benzoquinone. The oxidation from catecholate (CAT) to quinone (Q) is fully reversible and takes place via two consecutive one-electron processes; the intermediate between CAT and Q states is the radical anion semiquinone (SQ), Scheme 1.

Early work on the redox behavior of these coordinated ligands concerned the properties of dioxolene complexes of chromium, molybdenum, and tungsten.[5,6] Following initial work by Balch and Sohn using Ru^0 centers,[7] the Lever group carried out related studies on complexes containing Ru^{II}-based moieties coordinated to a variety of catechol derivatives.[8] Electrochemical studies on these systems revealed that although the redox couples for the CAT-SQ and SQ-Q processes were all at more negative potentials than the $Ru^{III/II}$ oxidation, the exact position of the ligand-centered processes varied depending on the ligand used. The same group has also studied the properties of similar complexes containing coordinated catechol derivatives with a range of O-, N-, and S-donor groups.[1f,9−12]

Building on the studies on mononuclear systems, the Ward group has synthesized a number of oligonuclear mixed valence systems containing catechol-type bridging ligands.[13] As they exhibit strong mixing of the metal and bridge molecular orbital, these complexes possess very rich redox chemistry with multiple accessible oxidation states.[14] Furthermore, because of the varied charge transfer states available to such systems, changes in oxidation state are often accompanied by large

Scheme 1. Catechol-Semiquinone-Quinone Redox Series

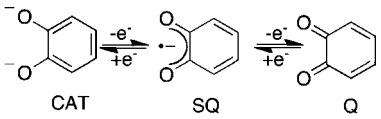

Received: April 20, 2011
Published: September 25, 2012

optical changes; this effect was exploited in the design of molecular devices for optical switching.[15]

Related to this topic, the Thomas and Félix groups have investigated the effect of a series of thiacrown ligands on the redox properties of ruthenium(II) centers[16,17] and used these fragments in the construction of mixed valence, MV, complexes.[18−22] Generally, it was found that, because of back bonding interactions involving overlap of C−S σ^* orbitals that are in-plane with occupied t_{2g} metal orbitals,[23] the thiacrowns stabilize the Ru^{II} state more than even polypyridyl ligands, and this effect increases as the number of S donors within the thiacrown increases. However, comparisons of MV systems containing macrocycles with the same number of S donors, revealed that changes in the size of the macrocycle also tune the intermetallic interaction and the overall redox chemistry of the entire system, presumably by changing the extent of the C−S σ^*/t_{2g} overlap. These Ru^{II}-thiacrown units have also been used to self-assemble novel mixed valence supramolecular architectures.[24,25]

This present study describes an initial investigation into the synthesis and behavior of ruthenium-dioxolene complexes that incorporate thiacrown-capped metal centers coordinated to catechol, 3,5-di-*tert*-butylcatechol (DTBC), and tetrachlorocatechol (TCC). In particular we wished to investigate whether the thiacrown ligands had any effect on the electrochemistry of the complexes when compared to the analogous bipyridine (bpy) and pyridine complexes. To assist the interpretation of the electrochemical and optical properties of these new complexes, theoretical studies involving density functional theory (DFT) calculations were also carried out.

RESULTS AND DISCUSSION

Synthetic Studies. In general, the reaction of the ruthenium-thiacrown precursors and catechol derivatives was accomplished by first reacting $[Ru([n]aneS_4)(DMSO)Cl]^+$ (n = 12, 14, 16)[16] with one mole equivalent of $AgNO_3$ in water/ethanol 1:1 at reflux for 1 h (see Experimental Section). Removal of AgCl by filtration yielded $[Ru([n]aneS_4)(OH_2)_2]^{2+}$ in solution. This was refluxed with one mole equivalent of catechol in the presence of the base 1,2,2,6,6-pentamethylpiperidine (pmp) for 2 h. It is known that thiacrown complexes are susceptible to nucleophilic attack by conventional bases;[26] therefore, pmp was used as it is a strong protic but non-nucleophilic base. Whereas the products of the reactions with catechol and DTBC (monocationic complexes $\mathbf{1}^+$−$\mathbf{6}^+$) were isolated as hexafluorophosphate salts, the reaction with TCC led to the precipitation of neutral complexes **7**−**9**.

Previous studies by Lever using the metal fragments $Ru^{II}(bpy)_2$ and $Ru^{II}(py)_4$ with the same three catechol ligands revealed that, although all the Ru^{II} complexes were isolated as neutral species with the dioxolene ligand in its CAT form, the complex $[Ru^{II}(bpy)_2DTBC]$ was rapidly aerially oxidized to the SQ form, with the sensitivity toward oxidation of the complexes increasing in the order TCC < catechol < DTBC.[8] When a $\{Ru^{II}([n]aneS_4)\}$ fragment is coordinated to the same ligands, only the TCC complexes are isolated as neutral diamagnetic species: NMR and MS studies confirm that all the catechol and DTBC complexes are paramagnetic cations. This suggests that complexes $\mathbf{1}^+$−$\mathbf{6}^+$ contain the ligand in their SQ form, whereas **7**−**9** are isolated in the CAT form (see Scheme 2).

Structural Studies. Yellow crystals of $[Ru([14]aneS_4)(TCC)]\cdot H_2O$ ($[\mathbf{8}]\cdot H_2O$) were grown by "reverse vapor diffusion" from dichloromethane and hexane. The crystal structure was determined by single crystal X-ray diffraction; selected bond lengths and angles are collected in Table 1. The significant structural features found in the solid state are shown in three different perspective views in Figure 1.

Scheme 2. Structure of the Complexes Synthesized in This Study

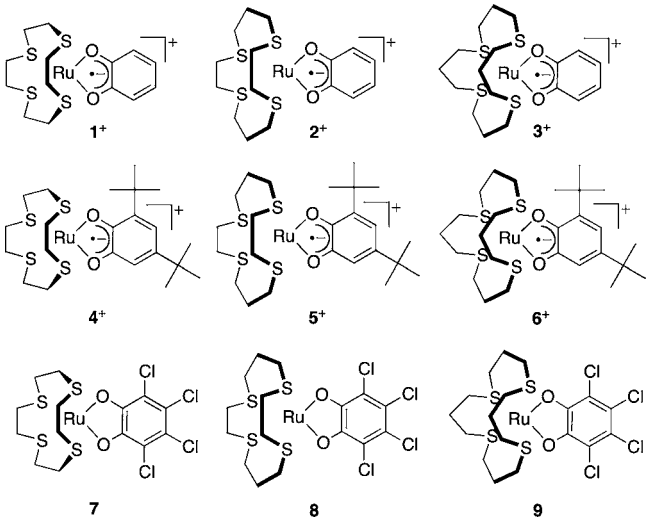

Table 1. Selected Bond Lengths and Angles for Complex $[\mathbf{8}]\cdot H_2O$

Bond Lengths [Å]			
Ru−S(1)	2.3307(9)	Ru−S(4)	2.2769(7)
Ru−S(2)	2.2767(6)	Ru−O(1)	2.109(2)
Ru−S(3)	2.354(1)	Ru−O(2)	2.116(2)
Angles [deg]			
O(1)−Ru−O(2)	79.84(5)		
S(1)−Ru−S(2)	99.14(4)	O(1)−Ru−S(3)	88.31(6)
S(1)−Ru−S(3)	176.71(4)	O(1)−Ru−S(4)	174.29(4)
S(1)−Ru−S(4)	86.31(4)	O(2)−Ru−S(1)	81.51(5)
S(2)−Ru−S(3)	84.15(5)	O(2)−Ru−S(2)	173.89(4)
S(2)−Ru−S(4)	91.45(2)	O(2)−Ru−S(3)	95.21(6)
S(3)−Ru−S(4)	93.75(5)	O(2)−Ru−S(4)	94.66(4)
O(1)−Ru−S(1)	91.32(6)		
O(1)−Ru−S(2)	94.06(4)		

The coordination sphere around the ruthenium center in complex **8** is a slightly distorted octahedron with the equatorial coordination plane defined by two sulfurs from $[14]aneS_4$ (S(2) and S(4)) and the oxygen donors of the TCC chelating ligand (see Figure 1, left). The remaining two macrocycle sulfur atoms (S(1) and S(3)) occupy the axial positions giving arise to an S(1)−Ru−S(3) axial angle of 176.71(4)°, which is deviated only 3.3° from the ideal value of a perfect octahedron (180°). Furthermore, the macrocycle adopts two alternative disordered folded conformations with unequal probability (see Experimental Section) which exhibit small differences in the S−C−C−S, S−C−C−C, and C−C−S−C endocyclic torsion angles.

The TCC ligand is tilted relative to the equatorial coordination plane (see Figure 1, left) leading to a dihedral angle between the [O(1),Ru,O(2)] and TTC (defined by their six carbon atoms) planes of 19.2° (ξ angle). This structural feature is unusual in six-coordinated Ru-TCC complexes as revealed by the distribution histogram calculated with data retrieved from Cambridge Structural Database, CSD,[27] and

dx.doi.org/10.1021/ic200814k | Inorg. Chem. 2012, 51, 10483−10494

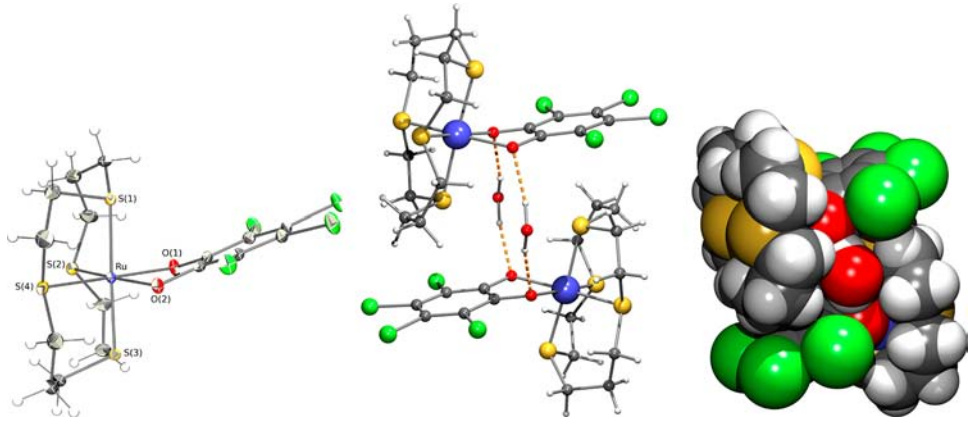

Figure 1. Diagrams showing different features of the crystal structure of [**8**]·H_2O: ORTEP view with labeling scheme adopted and thermal ellipsoids drawn at a 50% probability level (left); assembly of two [Ru([14]aneS_4)(TCC)] complexes through O···H−O hydrogen bonds established with two water molecules (center); space-filling model showing the close packing of the dimeric assembly (right).

presented in Supporting Information, Figure S1. In this histogram, the ξ angle ranges from 0.6 to 17.2° with a peak around 6°. However, the crystal packing of **8**·H_2O shows that two [Ru([14]aneS_4)(TCC)] molecules associate through O−H···O hydrogen bonds involving two water molecules and the TCC ligands (see Figure 1, center) with O···O distances of 2.901 Å and an O−H···O angle of 166°. In this centrosymmetric structure, the hydrogen bonds lead necessarily to a close packing of two [Ru([14]aneS_4)(TCC)] entities and the TCC ligands tilt relatively to the corresponding equatorial coordination plane to minimize the unfavorable steric interactions with methylene groups from the macrocycle of the adjacent [Ru([14]aneS_4)(TCC)] entity (see Figure 1, right).

Comparisons using data from the CSD,[27] reveal that the C−C and C−O bond lengths for the coordinated Cl_4-catechol ligand are similar to literature values for complexes containing the ligand in the reduced catecholate state. The coordination of TCC in a lower oxidation state than the catechol and DTBC ligands is consistent with previous results,[8] confirming that the chloro-groups of TCC act to stabilize the reduced CAT state by withdrawing electron density from the central dioxolene moiety.

Electrochemical Studies. For complexes **1**$^+$−**6**$^+$, cyclic voltammetry experiments were carried out in acetonitrile with 0.1 M Bu_4NPF_6 as the supporting electrolyte. The redox processes of complexes **1**$^+$−**6**$^+$ occur at similar potentials to those of their respective {Ru(bpy)$_2$} analogues (see Table 2).[8] Therefore, the Lever group's assignment of the redox processes can be applied with confidence. Processes at negative potential correspond to the dioxolene-centered SQ/CAT couple. The process at ∼ +0.6 V corresponds to the Q/SQ couple in every case, and a third process observed above +1.6 V can be assigned as a $Ru^{III/II}$ couple. For two of the complexes (complexes **4**$^+$ and **5**$^+$) this last couple is not observed, presumably because it is beyond the potential window of acetonitrile. For all the complexes, the two ligand-centered processes were fully chemically reversible, whereas the metal-centered processes that were observed displayed poor chemical reversibility. The SQ/CAT processes occur at a more negative potential for the complexes of DTBC. Again this is in agreement with previous results and indicates that, because of the electron-donating effect of the *tert*-butyl substituents, the SQ state of the coordinated DTBC is stabilized compared to that of catechol.

Table 2. Summary of Electrochemical Data for Complexes 1$^+$−9^{a,b}

complex	$E_{1/2}(1)$ (V)	$E_{1/2}(2)$ (V)	$E_{1/2}(3)$ (V)
1$^+$	−0.12	+0.64	+1.64[c]
2$^+$	−0.08	+0.72	+1.82[c]
3$^+$	−0.08	+0.77	+1.78[c]
4$^+$	−0.36	+0.52	*d*
5$^+$	−0.31	+0.61	*d*
6$^+$	−0.31	+0.64	+1.71[c]
7[e]	+0.13	+0.99	+1.80[c]
8[e]	+0.19	+1.09	+1.80[c]
9[e]	+0.15	+0.99	*d*

[a]Carried out under a dinitrogen atmosphere. Unless otherwise stated, support electrolyte: 0.1 M [NBu_4][PF_6] in MeCN, ν = 200 mV s^{-1} vs Ag/AgCl reference electrode. [b]Unless otherwise stated, couples are reversible with $\Delta E \leq 100$ mV and $|I_{Pa}/I_{Pc}| = 1$. [c]Couples are not chemically reversible therefore anodic peak potential quoted. [d]No $E_{1/2}(3)$ couples observed in this voltage window. [e]Support electrolyte: 0.1 M [NBu_4][PF_6] in dichloromethane.

The Q/SQ couples are also cathodically shifted for DTBC complexes compared to those of unsubstituted catechol.

A comparison of the $Ru^{III/II}$-redox potentials for **1**$^+$ to **3**$^+$ reveals that they are dependent on the nature of the thiacrown ligand coordinated to the metal center, with values varying by 180 mV. The redox potential for the ligand-centered processes is also dependent on the nature of the thiacrown. Like the metal-centered processes, ligand-centered couples for complex **1**$^+$ are more cathodic than those of **2**$^+$ and **3**$^+$, with differences between analogous couples ranging between 40 and 130 mV. A similar trend for ligand-centered couples is observed when complex **4**$^+$ is compared to **5**$^+$ and **6**$^+$: the relevant oxidation couples for the [12]aneS_4 complex are between 50 and 120 mV less positive than comparable oxidations for the other two complexes. These data are consistent with previous experimental and DFT studies showing that, because of its smaller coordination cavity, back-bonding interactions are weaker in [12]aneS_4 than in the larger thiacrowns,[17,20−22] which results in less stabilization of the Ru d(π) orbitals and hence less positive $Ru^{III/II}$ couples.

Complexes **7**−**9** were not soluble in acetonitrile, consequently dichloromethane with 0.1 M Bu_4NPF_6 was used as the supporting electrolyte for these systems and, as for the cationic complexes **1**$^+$−**6**$^+$, two chemically reversible processes

dx.doi.org/10.1021/ic200814k | *Inorg. Chem.* 2012, 51, 10483−10494

and one irreversible process at higher potential were observed for **7** and **8**. These are again assigned as the SQ/CAT, Q/SQ and Ru(III)/Ru(II) couples respectively. For complex **9** only two reversible couples are observed, presumably the third metal-based couple is outside the potential window of the support electrolyte. Interestingly, the effect of the size of thiacrown ligand on the potential of redox processes is less marked than for complexes $\mathbf{1}^+$–$\mathbf{6}^+$. Although the redox couples for complex **7**, which incorporates the [12]aneS$_4$ ligand, are still appreciably shifted with respect to **8**, (see Supporting Information, Figure S2) there is virtually no difference in the redox properties of **7** and **9**.

Absorption Spectroscopy Studies. For this technique, all the complexes were sufficiently soluble in acetonitrile. Spectra, recorded between 200–2000 nm (Table 3), were dependent on the nature of the catechol ligand coordinated to the metal center.

Table 3. UV/Visible Absorption Data for $\mathbf{1}^+$ to 9 in Acetonitrile

complex[a]	λ_{max} /nm (ε/dm^3 mol^{-1} cm^{-1})
$\mathbf{1}^+$	375 (2010); 617 (1080); 815(1120), 1035 (sh)
$\mathbf{2}^+$	350 (2680); 780 (1480), 1055 (sh)
$\mathbf{3}^+$	350 (1760); 640 (sh), 810 (1720)
$\mathbf{4}^+$	311 (4950), 360 (5020); 620 (sh), 760 (2450)
$\mathbf{5}^+$	315 (4140), 350 (sh), 600 (sh), 730 (1590), 895 (990)
$\mathbf{6}^+$	315 (7230); 350 (2205), 640 (sh), 775 (4620)
7	330 (6790); 460 (1140)
8	330 (7490), 400 (sh)
9	330 (9120); 460 (1720)

[a]Complexes $\mathbf{1}^+$–$\mathbf{6}^+$ were studied as hexafluorophosphate salts

For complexes $\mathbf{1}^+$–$\mathbf{6}^+$, absorption bands between 700 and 950 nm are observed. By comparison with similar systems these bands were tentatively assigned as charge transfer processes between the metal centers and relatively electron-deficient SQ-forms of the dioxolene ligands. A comparison of the energy of this band between complexes with the same dioxolene ligand reveals that it is dependent on the nature of the thiacrown ligand coordinated to the metal center. In both the $\mathbf{1}^+$–$\mathbf{3}^+$ series and the $\mathbf{4}^+$–$\mathbf{6}^+$ series, the band energy is highest for the [14]aneS$_4$-based complex. Again, this trend is also consistent with previous work[20–22] showing that [14]aneS$_4$ is most preorganized to bind to octahedral centers with the minimum of steric strain. This stabilization of the Ru^{II}[14]aneS$_4$ unit, which supplies the occupied orbitals for the Ru^{II}→SQ charge-transfer, results in the observed shift to lower wavelength of the low energy band. Indeed a comparison of the metal-based oxidations within the $\mathbf{1}^+$–$\mathbf{3}^+$ series is also consistent with this interpretation, as $\mathbf{2}^+$ displays the most anodic oxidation. Complexes $\mathbf{1}^+$–$\mathbf{6}^+$ also display intense absorptions at higher energies that were assigned with the aid of time-dependent DFT (TD-DFT) calculations, vide infra.

As expected, the neutral complexes **7**–**9**, which contain the TCC ligand in the reduced CAT state, do not possess the same lower energy bands observed for $\mathbf{1}^+$–$\mathbf{6}^+$. Although all nine complexes display intense high-energy transitions at approximately 330 nm, the bands for complexes **7**–**9** are notably more intense than those observed for complexes $\mathbf{1}^+$–$\mathbf{6}^+$, suggesting that they contain contributions from additional transitions. This hypothesis is supported by consequent TD-DFT calculations described below.

Spectroelectrochemical Studies. Complexes were studied using UV/vis/NIR spectroelectrochemistry. It transpired that only complexes $\mathbf{2}^+$, $\mathbf{5}^+$, and **8** were sufficiently stable to probe the entire CAT/SQ/Q redox chain on the slow timescale of spectroelectrochemistry and produce a final spectrum that was identical to the initial spectrum after restoring the applied potential to its initial value. Furthermore, to ensure good solubility of the complexes in all three oxidation states studied, the experiments were carried out in dichloromethane at 273 K.

Since the isolated state of complex $\mathbf{2}^+$ is the SQ state, the first oxidation (SQ→Q) and the single reduction processes (SQ→CAT) were analyzed. Oxidation of the complex at +1.25 V results in the changes shown in Figure 2A. The broad Ru^{II}→SQ MLCT, observed between 650–1200 nm, increase in intensity upon oxidation accompanied by a 25 nm blue shift in λ_{max} to 755 nm ($\Delta\nu$ = 425 cm^{-1}). Although the SQ→Q oxidation process lowers the π^* of the ligand, it seems that greater mixing of this orbital with metal based orbital actually results in a hypsochromic shift, a phenomenon that has been observed before.[8] As expected, reduction of $\mathbf{2}^+$ at −0.75 V, which would be expected to generate the CAT-state, causes the metal-to-ligand charge-transfer (MLCT) transition to collapse (Figure 2B), resulting in a final unchanging spectrum bearing a strong resemblance to the spectra of complexes **7**–**9**, which are also

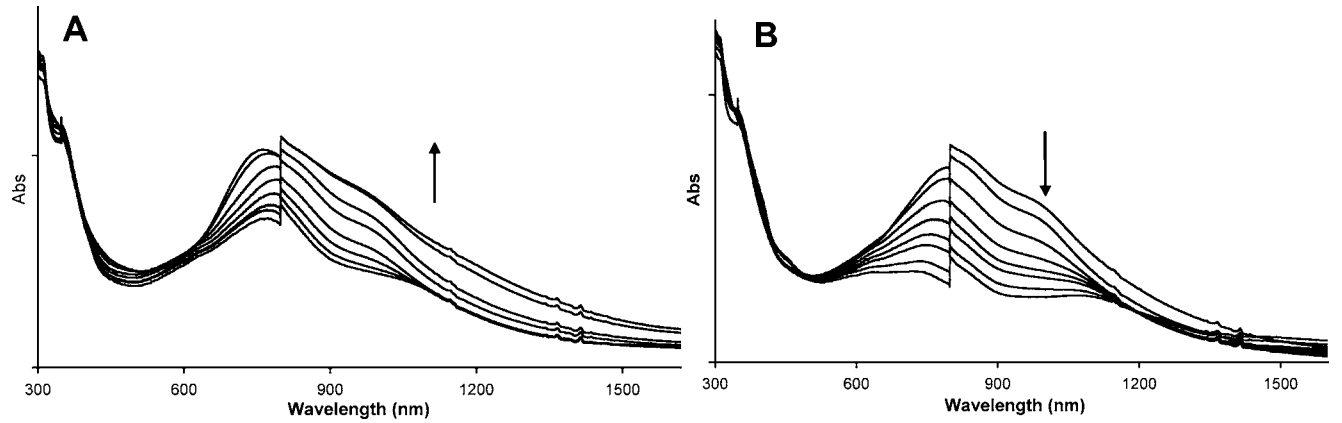

Figure 2. (A) Change in absorption spectrum of complex $\mathbf{2}^+$ upon single electron oxidation. (B) Change in absorption spectrum of complex $\mathbf{2}^+$ upon one electron reduction. The discontinuity at 800 nm is due to a detector change on the spectrometer.

dx.doi.org/10.1021/ic200814k | Inorg. Chem. 2012, 51, 10483–10494

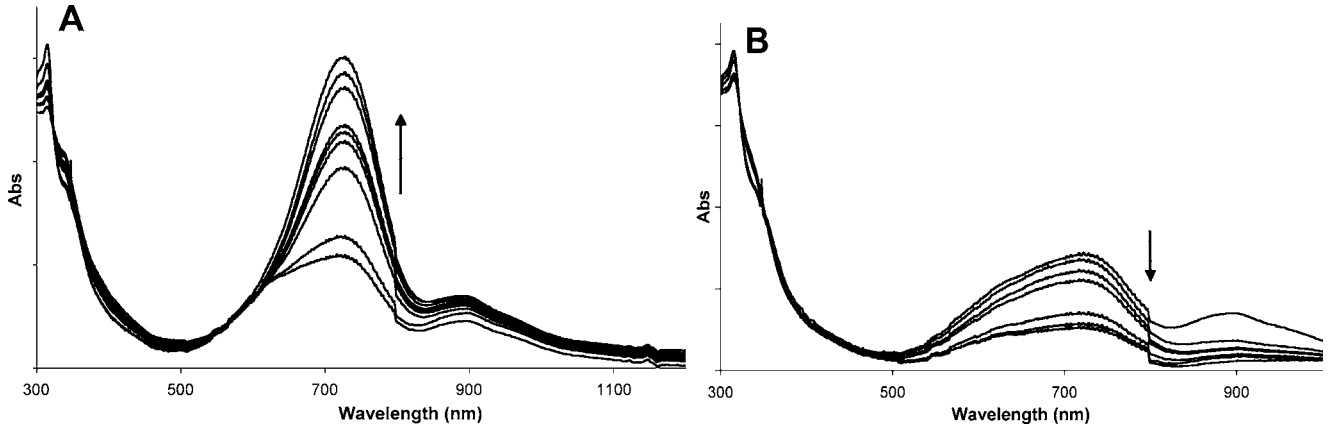

Figure 3. (A) Change in absorption spectrum of complex 5^+ upon one electron oxidation (SQ→Q). (B) Change in absorption spectrum of complex 5^+ upon one electron reduction (SQ→CAT). The discontinuity at 800 nm is due to a detector change on the spectrometer.

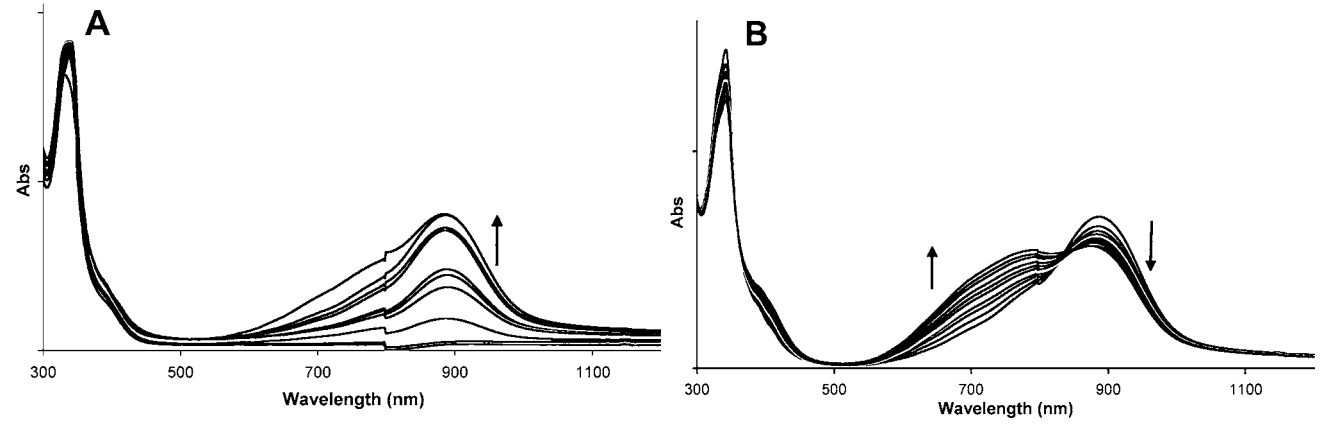

Figure 4. (A) Change in absorption spectrum of complex **8** upon its first one electron oxidation (CAT→SQ). (B) Changes for the second one electron oxidation of the complex (SQ→Q). The discontinuity at 800 nm is due to a detector change on the spectrometer.

fully reduced. Although the final spectrum does not fully collapse, higher negative potentials produce no further changes in the observed spectra, and return to 0 V again regenerates a spectrum that was superimposable on the original for 2^+. It is possible that the sample contains a small amount of impurity that causes the final absorbances, which seems unlikely as the characterization data indicates that it is pure. Alternatively, despite vigorous purging, the spectroelectrochemical cell may have still contained a trace of oxygen that reoxidized the reduced species. Nevertheless, it is clear that the MLCT band collapses (if not fully), and this change is consistent with the generation of the CAT state, a postulate that agrees with DFT calculations (vide infra).

Although oxidation of complex 5^+ at +1.0 V produces more pronounced intensity changes than the ones observed for 2^+, there is a negligible shift in the MLCT band (<3 nm), see Figure 3A. Again, as for 2^+, reduction of 5^+ at −0.75 V to the CAT state of the ligand resulted in the expected reduction in the MLCT band producing the final spectrum shown in Figure 3B.

Complex **8** is isolated with the coordinated TCC ligand in its CAT state; consequently spectroelectrochemical studies on this system involved two sequential single electron oxidations. Oxidation of the complex at +0.65 V resulted in the growth of a moderately intense absorption band at 890 nm (Figure 4A), which is comparable in energy to bands observed in the electronic spectra of complexes 1^+−6^+; thus, this transition is assigned to Ru^{II}→SQ MLCT.

On further oxidation of the complex to the dioxolene Q state, the band at 890 nm is diminished in intensity, and a new peak at 790 nm, assigned to the Ru^{II} → Q MLCT, grows in ($\Delta\nu$ = 1425 cm^{-1}). These changes are associated with an isosbestic point at 835 nm, Figure 4B. A comparison with the analogous optical changes that occur during the oxidation of 2^+ and 5^+ reveals that the difference in energy between the Ru^{II}→SQ and Ru^{II}→Q transitions of $8^+/8^{2+}$ are appreciably larger than those observed for the other two complexes and, as expected, this trend mirrors the ease of the oxidation of the individual complexes.

Computational Studies. To provide further insights into the experimental data, DFT calculations were performed on complexes 1^+−3^+ and **7**−**9**. These complexes were chosen because they allow us to study the effect of both the dioxolene ligand type and the size of the thiacrown. As the crystal structure of **8** is available, initially, the molecular structure of this complex was energy minimized in gas-phase by DFT (B3LYP)[28] using the LANL2TZ(f)[29] basis set for Ru and 6-311G*[30] for the remaining elements, apart from sulfur. Since the reproduction of the experimental Ru−S bond lengths proved to be challenging, several basis sets for S were tested. The tested basis sets are listed in Supporting Information, Table S1 together with the corresponding Ru−S optimized bond lengths. In fact, all basis sets led to Ru−S bonds[31]

dx.doi.org/10.1021/ic200814k | Inorg. Chem. 2012, 51, 10483−10494

systematically longer than those obtained experimentally, a general trend that had been observed in our previous work.[22] However, since the aug-cc-pVQZ basis set[32] gave the smallest deviations from the experimental data it was selected for subsequent calculations. We then reoptimized complex **8** solvated in acetonitrile through a polarizable continuum model (see computational details below) using this basis set.

The Supporting Information, Table S2 contains the solution optimized DFT bond lengths (Å) and angles (deg) in the ruthenium coordination sphere of complex **8**, while Figure 5

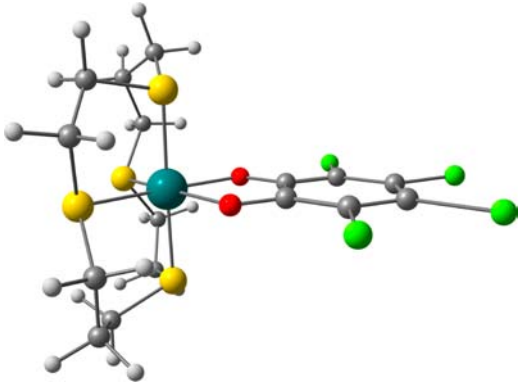

Figure 5. DFT optimized structure of complex **8** with the ξ tilt angle of 0.2°. Carbon atoms are shown in gray, hydrogen atoms in white, sulfur atoms in yellow, oxygen atoms in red, chloride atoms in green, and ruthenium atom in blue.

depicts the DFT optimized structure. The rms (root-mean-square) between optimized and X-ray structure is 0.414 Å (excluding the hydrogen atoms), with the main experimental structural features being retained, including the slightly distorted octahedral coordination geometry. The bond lengths at the ruthenium center agree very well, the largest deviation being 0.063 Å for the Ru−S(4) bond, although the Ru−S lengths are systematically longer than the experimental ones, as mentioned earlier. The Ru−O bond lengths also agree very well and the main bond angles are reproduced, with the higher deviation found for the O(2)−Ru−S(3) *cis* angle (4.8°). However, the remarkable tilt of the TCC ligand found in the crystal structure, given by the ξ angle (vide supra) is not reproduced.

Indeed, the ξ angle in **8**·H_2O is 19.2°, whereas the DFT optimized value is only ∼0° showing that the TCC ligand is coplanar with the equatorial sulfur donor atoms. However this large deviation is understandable taking into account that, as mentioned above, the ξ angle in the X-ray structure seems to be dictated by crystal packing effects, in particular, the interaction with the water molecules. Since this effect should not be important in solution, the calculated structure should be a reliable model, as corroborated by the subsequent TD-DFT calculations outlined below.

The structure of complex **8** was used as starting point to generate the initial geometries of complexes $\mathbf{1}^+$−$\mathbf{3}^+$, **7**, and **9**, which were subsequently optimized by DFT in acetonitrile solution. Their main geometric parameters are also reported in Supporting Information, Table S2. All the structures present a similar slightly distorted octahedral coordination environment, and their ξ angles are very close to 1° as calculated in **8**.

The calculated electronic structures of $\mathbf{1}^+$−$\mathbf{3}^+$ reveal that their β-LUMOs are mainly located at the dioxolene ligands. There is however a considerable contribution from the metal (Ru-dioxolene π^*), ranging from ∼10% in $\mathbf{2}^+$ and $\mathbf{3}^+$ to 26% in $\mathbf{1}^+$. The corresponding singly occupied molecular orbitals (SOMOs) (α) are very similar with Ru contributions around 18% for $\mathbf{2}^+$ and $\mathbf{3}^+$ whereas in $\mathbf{1}^+$ the metal contribution is relatively high (29%). Clearly the size of the macrocycle influences the mixing of the SQ orbitals with Ru, this mixing being particularly important in $\mathbf{1}^+$ with [12]aneS_4 . This effect is also observed in complexes **7**−**8** highest occupied molecular orbitals (HOMOs): whereas for **8** and **9**, they are indeed mainly localized in the TCC ligand with some mixing with Ru (∼16%), in **7** the metal contribution is ∼25%. These MO compositions can be found in Supporting Information, Tables S3−S8.

Using the optimized structures, we performed TD-DFT calculations with acetonitrile as solvent using a polarizable continuum model (see computational details below), and the relevant excitations are listed in Tables 4 and 5. To assist the assignment of the experimental bands and to visualize the agreement between the calculated spectra and the experimental ones, Figures 6 and 7 show the experimental UV/Visible absorption spectra superimposed with all the calculated excitations in acetonitrile.

First of all, it should be emphasized that the calculation of accurate excitation energies of open-shell molecules like $\mathbf{1}^+$−$\mathbf{3}^+$ is inherently difficult at the linear-response TD-DFT level of theory[33] and, as pointed out by Casida and co-workers,[34] one should only trust those states which preserve the expectation

Table 4. Most Relevant TD-DFT Excitation Energies (λ), Compositions, and Oscillator Strengths (OS) for Complexes $\mathbf{1}^+$−$\mathbf{3}^+$ Compared with Experimental Data (λ_{exp})[a]

complex	excitation no.	λ (nm)	OS	composition	λ_{exp} (ε/dm^3 mol^{-1} cm^{-1})	assignment
$\mathbf{1}^+$	2	820	0.016	H-2(β) → LUMO(β) (61%)	1035 (sh)	MLCT
				H-1(β) → LUMO(β) (38%)		
	3	724	0.147	H-1(β) →LUMO(β) (61%)	815 (1120)	MLCT
				H-2(β) → LUMO(β) (37%)		
	6	531	0.004	H-3(β) → LUMO(β) (96%)	617 (1080)	MLCT, π−π^*
$\mathbf{2}^+$	2	877	0.001	H-1(β) → LUMO(β) (99%)	1055 (sh)	MLCT
	3	706	0.111	H-2(β) → LUMO(β) (99%)	780 (1480)	MLCT
$\mathbf{3}^+$	2	949	0.000	H-1(β) → LUMO(β) (99%)		MLCT
	3	720	0.122	H-2(β) → LUMO(β) (98%)	810 (1720)	MLCT
	4	588	0.004	H-3(β) → LUMO(β) (97%)	640 (sh)	MLCT, π−π^*

[a]The full list of calculated excitations is given in Supporting Information, Tables S9−S11. MO compositions are given in Supporting Information, Tables S3−S5. MO pictures are given in Supporting Information, Figures S3−S5.

dx.doi.org/10.1021/ic200814k | *Inorg. Chem.* 2012, 51, 10483−10494

Table 5. Most Relevant TD-DFT Excitation Energies (λ), Compositions, and Oscillator Strengths (OS) for Complexes 7−9 Compared with Experimental Data (λ_{exp})[a]

complex	excitation n°	λ (nm)	OS	composition	λ_{exp} (ε/dm^3 mol^{-1} cm^{-1})	assignment
7	1	520	0.014	HOMO → LUMO (80%)	460 (1140)	LLCT/LMCT
	9	332	0.070	HOMO → L+3 (91%)		
	13	308	0.078	HOMO → L+7 (52%)		
				H-1 → L+1 (35%)		
	15	303	0.084	H-1 → L+1 (58%)	330 (6790)	LLCT and Ru→TCC MLCT
				HOMO→L+7 (29%)		
8	1	445	0.0105	HOMO → L+1 (47%)	400sh	LLCT/LMCT
				HOMO → LUMO (34%)		
				H-3 → L+1 (12%)		
	9	319	0.067	HOMO → L+4 (65%)		
				HOMO → L+3 (28%)		
	14	302	0.074	HOMO → L+5 (48%)	330 (7490)	LLCT and Ru→TCC MLCT
				H-1 → L+3 (21%)		
				H-1 → L+2 (16%)		
9	1	446	0.008	HOMO → L+1 (55%)	460 (1720)	LLCT/LMCT
				HOMO → LUMO (22%)		
				H-3 → L+1 (16%)		
	8	322	0.083	HOMO → L+3 (55%)	330 (9120)	LLCT and Ru→TCC MLCT
				H-1 → LUMO (30%)		
	9	319	0.061	H-1 → LUMO (54%)		
				HOMO → L+3 (28%)		

[a]The full list of calculated excitations can be found in Supporting Information, Tables S12−S14. MO compositions are given in Supporting Information, Tables S6−S8. MO pictures are given in Supporting Information, Figures S6−S8.

value of $\langle\hat{S}^2\rangle$, that is, $\Delta\langle\hat{S}^2\rangle \approx 0$. Values of $\Delta\langle\hat{S}^2\rangle \approx 2$ indicate excitation to an nonphysical state, while $\Delta\langle\hat{S}^2\rangle \approx 1$ correspond to an excitation that is too spin contaminated and should be discarded even though they could present considerable oscillator strengths. In this work, only excitations with $\Delta\langle\hat{S}^2\rangle \approx 0$ were considered in the analysis. Our results show that, as the energies increase, the excitations are less trustworthy (see Supporting Information, Tables S9−S11). Therefore, the TD-DFT results will only be used to assign the low-energy bands of the experimental spectra.

In complexes $\mathbf{1}^+$−$\mathbf{3}^+$ the calculated low-energy excitations agree qualitatively with the experimental absorptions (see Figure 6 and Table 4). Clearly, the calculated spectra are all blue-shifted compared to the experimental data.

For $\mathbf{1}^+$ the first experimental band at 815 nm, corresponds to the calculated excitation at 724 nm. According to the change of electron density shown in Figure 8 this excitation is a charge transfer from the metal to the SQ ligand, MLCT. Experimentally, there is also a shoulder at 1035 nm, which appears as a calculated excitation at 820 nm (excitation 2). Here, the agreement is very poor, given the relative oscillator strengths (excitation 3 vs excitation 2) and the difference between the calculated wavelength and the experimental value. This transition is also assigned as MLCT (see Figure 8). The experimental band at 617 nm is also badly reproduced, since the corresponding calculated excitation appears at 531 nm, but with very low oscillator strength; nevertheless, it is also consistent with a MLCT with increasing π−π^* character. At higher energies the excitations are too spin contaminated to be trusted.

Complexes $\mathbf{2}^+$ and $\mathbf{3}^+$ behave similarly. Again, low-energy transitions with relatively strong oscillator strengths are calculated at 706 and 720 nm, respectively, which are in modest agreement with the experimental bands observed at 780 and 810 nm. Both are assigned, according to the change of electron density upon excitation represented in Figures 9 and 10, as Ru → SQ charge transfer (MLCT). The recorded spectrum of $\mathbf{2}^+$ also presents a shoulder at 1055 nm, which was calculated at 877 nm, with very low oscillator strength (0.001, not shown in Figure 6). This transition is also MLCT (Figure 9) and was estimated to occur at 949 nm for $\mathbf{3}^+$, although experimentally in this case it is not observed (which agrees with the calculated OS of 0.000). For this complex an experimental shoulder appears at 640 nm, which was calculated at 588 nm (excitation 4, not shown in Figure 6). This is the same transition responsible for the experimental band at 617 nm in complex $\mathbf{1}^+$ and is also assigned as a mixture of MLCT with π−π^* (Figure 10). Again, although the agreement between the calculated OS and the experimental intensity is poor, the qualitative assignments should be correct. The higher energy excitations were also not considered.

A similar analysis on the TCC-based complexes **7**−**9** was also carried out. The calculated excitations are in moderate agreement with the experimental spectra (see Figure 7) although some spectral trends are not fully reproduced (vide infra). Experimentally, the major spectral difference for these complexes compared to their SQ counterparts ($\mathbf{1}^+$−$\mathbf{3}^+$) is the lack of low-energy MLCT bands around 700−950 nm, and our TD-DFT calculations mirror these results since no excitations were calculated in this spectral region.

The first low-energy transitions are calculated at 520 nm, 445 nm, and 446 nm (see Table 5 and Figure 7) with oscillator strengths around 0.01 for **7**, **8**, and **9**, respectively, in good agreement with the experimental ones (460 nm, 400 and 460 nm). However, it should be noted that the trend in the energies for this absorption (**8** > **7** = **9**) was not properly reproduced by our TD-DFT calculations (**8** ≈ **9** > **7**), and, the transition for complex **7** in particular has a lower calculated energy. These transitions involve, as shown in Figures 11, 12, and 13 (left), the occupied TCC centered orbitals (green) and empty metal−

dx.doi.org/10.1021/ic200814k | Inorg. Chem. 2012, 51, 10483−10494

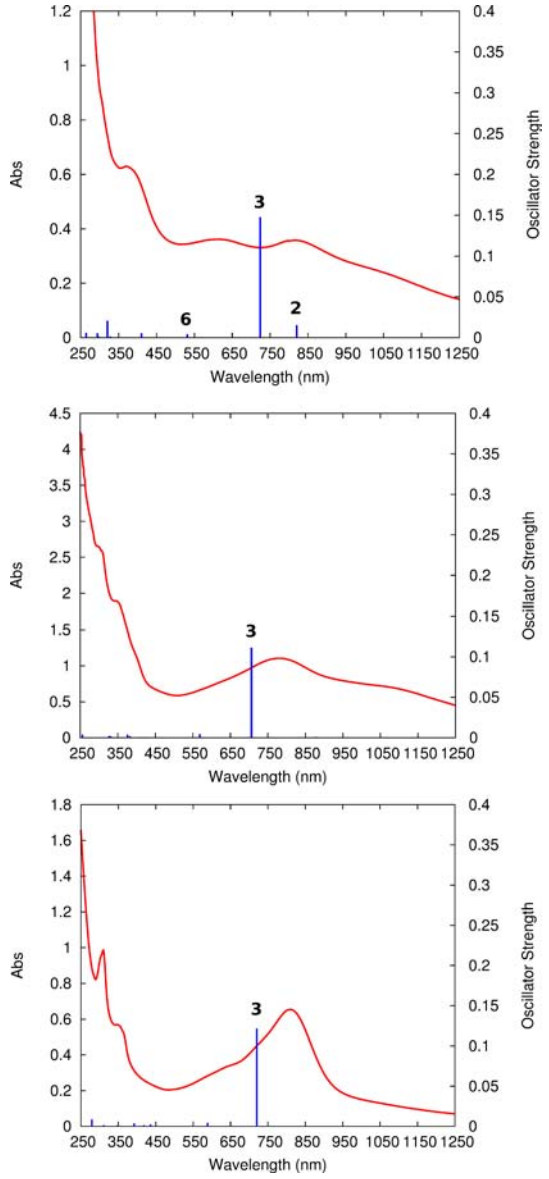

Figure 6. Calculated TD-DFT excitations (blue) plotted against the UV/Visible absorption spectra (red) for complexes $\mathbf{1}^+$ (top), $\mathbf{2}^+$ (center), and $\mathbf{3}^+$ (bottom). The black bold numbers correspond to the excitation number (a full list is provided in Supporting Information, Tables S9–S11).

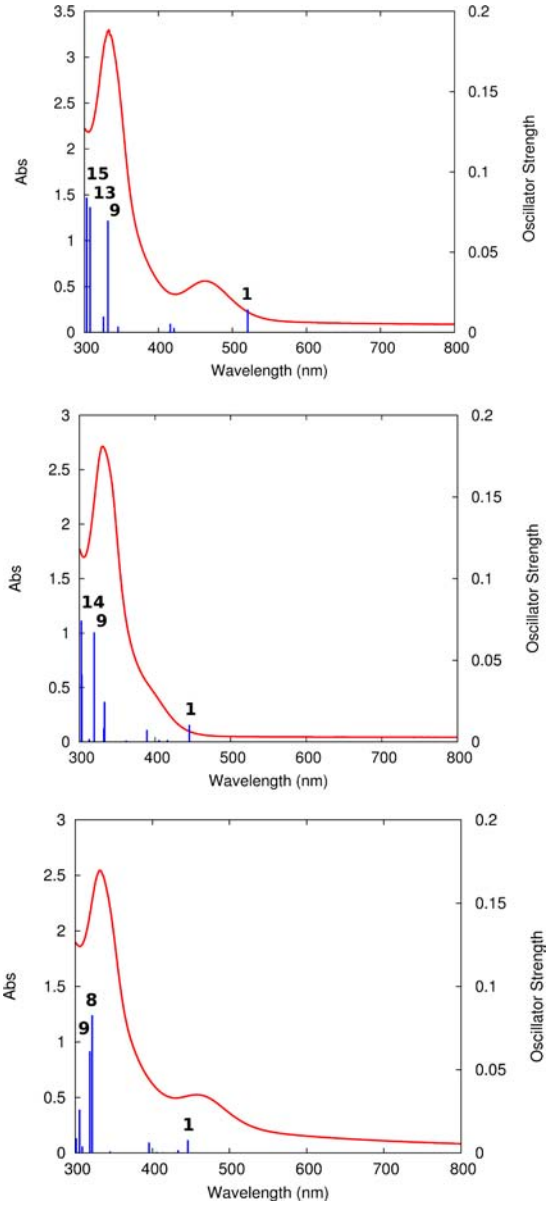

Figure 7. Calculated TD-DFT excitations (blue) plotted against the UV/Visible absorption spectra (red) for complexes **7** (left), **8** (center), and **9** (right). The black bold numbers correspond to the excitation number (a full list is provided in Supporting Information, Tables S12–S14).

sulfur σ^* (black) orbitals, being assigned as a mixture of LLCT and LMCT.

At lower wavelengths, the TD-DFT spectra are dominated by other absorptions that are absent in complexes $\mathbf{1}^+$–$\mathbf{3}^+$. These excitations have higher oscillator strength (>0.06), the stronger ones being calculated at 303 nm, 302 nm, and 322 nm for **7**, **8**, and **9**, respectively, which, together with the other strong excitations in that area, correspond to the high-energy experimental bands found at 330 nm. Again, the agreement is acceptable. These high-energy bands should correspond, according to Figures 11, 12, and 13, to the depletion of charge of the TCC ligand and metal, transferring it into the C–S σ^* orbitals of the thiacrown (LLCT and MLCT), with some mixture of TCC intraligand transitions.

■ CONCLUSIONS

The redox-active dioxolene ligands catechol, 3,5-di-*tert*-butylcatechol, and tetrachlorocatechol were successfully coordinated to ruthenium centers also containing one of the tetradentate thiacrown ligands [12]aneS$_4$, [14]aneS$_4$, and [16]aneS$_4$, yielding complexes **1**–**9**. A range of analytical and computational techniques confirmed that in those complexes containing tetrachlorocatechol, the ligand was in the reduced catecholate (CAT) state in the ground state. For both the catechol and 3,5-di-*tert*-butylcatechol based complexes the ligands were in the one-electron oxidized semiquinonate (SQ) state, although the catechol complexes were easier to reduce than their DTB-catechol analogues, results that are in agreement with the behavior of the ligands in octahedral analogous {Ru(bpy)$_2$} complexes. Spectroelectrochemical

dx.doi.org/10.1021/ic200814k | *Inorg. Chem.* 2012, 51, 10483–10494

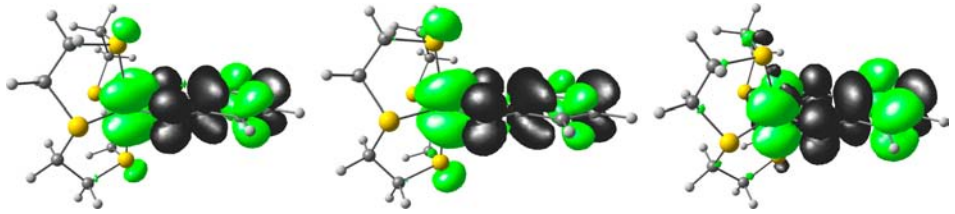

Figure 8. Change of electron density for complex 1^+ upon the excitations 2, 3, and 6 (left to right) as defined in Table 4. Green and black correspond to a decrease and increase of electron density, respectively.

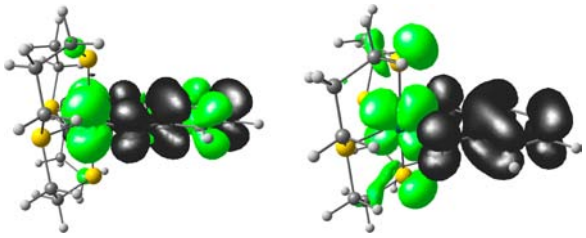

Figure 9. Change of electron density for complex 2^+ upon the excitations 2 (left) and 3 (right) as defined in Table 4.

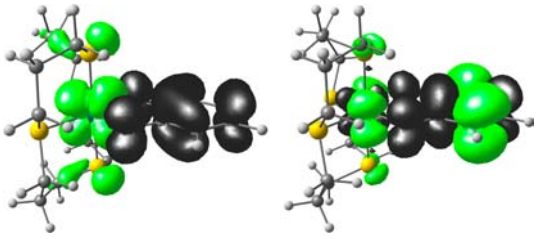

Figure 10. Change of electron density for complex 3^+ upon the excitations 3 (left) and 6 (right) as defined in Table 4.

studies on the ligand-centered processes of several of the complexes showed the consistent growth and collapse of characteristic Ru →dioxolene MLCT bands when the ligands were in oxidized SQ or Q states. Comparison of the MLCT peaks shows that the presence of the electron-withdrawing and donating substituents effects a change in energy of the respective transitions. In TCC-based complexes **7**, **8**, and **9**, a transition assigned as LLCT from TCC to the thiacrown macrocycle occurring at higher energies is experimentally observed, and this assignment is confirmed by TD-DFT calculations.

Although comparisons of the effect of thiacrown size on the electrochemistry of the complexes indicated that the smaller crown, [12]aneS$_4$, had a small stabilizing effect on the more reduced forms of the catecholate ligands, shifting the redox potentials compared to the complexes of the larger crowns, the spectroelectrochemical studies on these mononuclear complexes indicate that the electronic properties of these systems are not qualitatively affected by the variation in the structure of the coordinated thiacrown.

The synthetic routes outlined in this study can be extended to produce related oligonuclear complexes. The electrochemically switchable optical properties of analogous dinuclear {Ru^{II}(bpy)$_2$} systems have already provided the basis of a prototypical electrochromic device.[15] With the aim of creating similar devices with modulated switching responses or differing switchable optical windows, studies on the synthesis, electrochemical and optical properties of similar thiacrown analogues will form the basis of future reports.

EXPERIMENTAL SECTION

Materials. All chemicals were obtained from commercial sources and were used as supplied unless otherwise stated. The complexes [RuCl(DMSO)([*n*]aneS$_4$)][PF$_6$] (*n* = 12,14,16) were synthesized using published methods.[17] Solvents were obtained from commercial sources and were dried and purified using standard literature method. All reactions were carried out under a nitrogen atmosphere unless otherwise stated.

Physical Measurements. Microanalyses for carbon, hydrogen, nitrogen, and sulfur were obtained using a Perkin-Elmer 2400 analyzer, working at 975 °C. ^{1}H NMR spectra were recorded on a Bruker AM250 machine. Mass spectra were obtained on a Kratos MS80 instrument in positive ion mode with a *m*-nitrobenzyl alcohol matrix. UV/vis spectra were recorded on a Unicam UV/vis UV2 spectrometer in twin beam mode. Cyclic voltammetry was carried out using an EG&G Versastat III potentiostat. Measurements were made using approximately 2×10^{-3} mol dm^{-3} solutions in dry solvents under a nitrogen atmosphere, with support electrolyte as stated. Potentials were measured with reference to a Ag/AgCl (saturated AgCl in saturated KCl) electrode at a sweep rate of 200 mV s^{-1}. In the conditions used the ferrocene/ferrocenium couple was observed at 400 mV (ΔE_p = 60 mV). UV/vis/NIR spectroelectrochemical measurements were performed on a Cary 5000 spectrophotometer in dichloromethane using an OTTLE cell thermostatted at 273 K unless stated otherwise.

Syntheses. *[1](PF$_6$).* [Ru([12]aneS$_4$)(DMSO)Cl](PF$_6$) (200 mg, 0.33 mmol) and AgNO$_3$ (57 mg, 0.33 mmol) were refluxed in 20 cm^3 of ethanol/water 1:1 for 1 h. After removal of precipitated AgCl by filtration, catechol (40 mg, ~1.1 equivalents) was added along with 1,2,2,6,6-pentamethylpiperidine (0.5 cm^3, excess), and the mixture refluxed for 2 h. Upon cooling, a small amount of precipitate formed, this was removed by filtration. Excess NH$_4$PF$_6$ (163 mg, 3 equivalents) was added to the filtrate, and the ethanol removed in vacuo. The

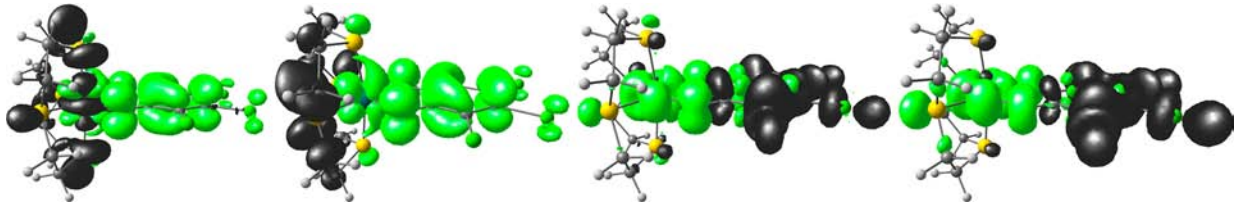

Figure 11. Change of electron density for complex **7** upon the excitations 1, 9, 13, and 15 (left to right) as defined in Table 5.

dx.doi.org/10.1021/ic200814k | *Inorg. Chem.* 2012, 51, 10483−10494

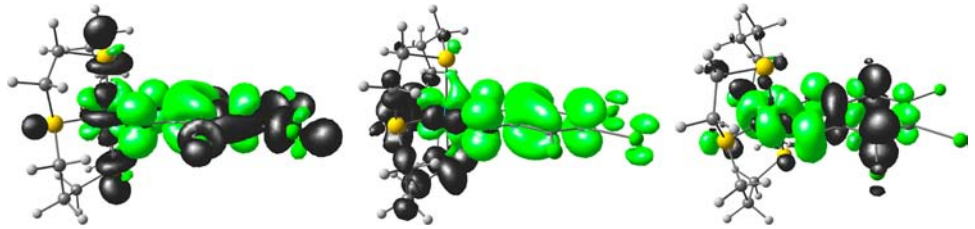

Figure 12. Change of electron density upon the excitation 1 (left), 9 (center), and 14 (right) for complex **8**. The color scheme is given in Figure 8.

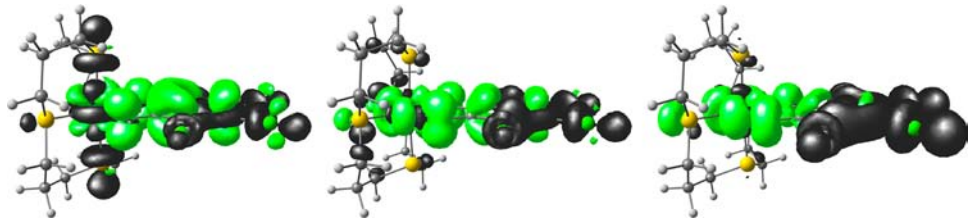

Figure 13. Change of electron density upon the excitation 1 (left), 8 (center), and 9 (right) for complex **9**. The color scheme is given in Figure 8.

resulting blue-green precipitate was collected, washed with water and ethanol, and dried in vacuo. Mass: 180 mg (0.30 mmol, 91%). ESI-MS; m/z = 450 [M^+ - PF_6]. Accurate Mass MS: Calculated for $C_{14}H_{20}O_2RuS_4$ [M^+ - PF_6]: 449.9390. Found: 449.9390 ± 0.2 PPM. Elemental Analysis: $C_{14}H_{20}F_6O_2PRuS_4$: calcd. C, 28.28; H, 3.39; found C = 28.43%, H = 3.61%.

[2](PF$_6$). This was synthesized using the same procedure as [**1**](PF_6), but with the following differences: [Ru([14]aneS_4)(DMSO)Cl](PF_6) (388 mg, 0.62 mmol), $AgNO_3$ (105 mg, 0.62 mmol), and 75 mg of catechol were used. The resulting blue-green precipitate was collected, washed with water and ethanol, and dried in vacuo. Mass: 259 mg (0.42 mmol, 67%). ESI-MS; m/z = 478 [M^+-PF_6]. Accurate Mass MS: Calculated for $C_{16}H_{24}O_2RuS_4$ [M^+ - PF_6]: 477.9703. Found: 477.9727 ± 2.2 PPM. Elemental Analysis: $C_{16}H_{24}F_6O_2PRuS_4$: calcd. C, 30.86; H, 3.89; found C = 30.47%, H = 3.53%.

[3](PF$_6$). This was synthesized using the same procedure as [**1**](PF_6), but with the following differences: [Ru([16]aneS_4)(DMSO)Cl](PF_6) (150 mg, 0.23 mmol), $AgNO_3$ (38.9 mg, 0.23 mmol) and 28 mg of catechol were used were used. The resulting blue-green precipitate was collected, washed with water and ethanol, and dried in vacuo. Mass: 68 mg (0.10 mmol, 45%). ESI-MS; m/z = 506 [M^+ - PF_6]. Accurate Mass MS: Calculated for $C_{18}H_{28}O_2RuS_4$ [M^+ - PF_6]: 506.0016. Found: 506.0024 ± 3.0 PPM. Elemental Analysis (for [**3**](PF_6)·H_2O): $C_{18}H_{30}F_6O_3PRuS_4$: calcd. C, 32.33; H, 4.52; found C = 32.55%, H = 4.40%.

[4](PF$_6$). This was synthesized using the same procedure as [**1**](PF_6), but with the following differences: [Ru([12]aneS_4)(DMSO)Cl](PF_6) (200 mg, 0.33 mmol), $AgNO_3$ (57 mg, 0.33 mmol), and 74 mg of 3,5-di-*tert*-butylcatechol were used. The resulting turquoise precipitate was collected, washed with water and ethanol, and dried in vacuo. Mass: 73 mg (0.10 mmol, 31%). Accurate Mass MS: Calculated for $C_{22}H_{36}O_2RuS_4$ [M^+ - PF_6]: 562.0642. Found: 562.0640 ± 0.2 PPM. Elemental Analysis: $C_{22}H_{36}F_6O_2PRuS_4$: calcd. C, 37.38; H, 5.13; found C = 37.79%, H = 4.95%.

[5](PF$_6$). This was synthesized using the same procedure as [**1**](PF_6), but with the following differences: [Ru([14]aneS_4)(DMSO)Cl](PF_6) (209 mg, 0.33 mmol), $AgNO_3$ (57 mg, 0.33 mmol) and 74 mg of 3,5-di-*tert*-butylcatechol were used. The resulting turquoise precipitate was collected, washed with water and ethanol, and dried in vacuo. Mass: 117 mg (0.16 mmol, 48%). Accurate Mass MS: Calculated for $C_{24}H_{40}F_6O_2RuS_4$ [M^+ - PF_6]: 590.0955. Found: 590.0980 ± 4.3 PPM. Elemental Analysis (for [**5**](PF_6)·2H_2O): $C_{24}H_{44}F_6O_4PRuS_4$: calcd. C, 37.39; H, 5.75; found C = 37.30%, H = 5.52%.

[6](PF$_6$). This was synthesized using the same procedure as [**1**](PF_6), but with the following differences: [Ru([16]aneS_4)(DMSO)Cl](PF_6) (218 mg, 0.33 mmol), $AgNO_3$ (57 mg, 0.33 mmol), and 74 mg of 3,5-di-*tert*-butylcatechol were used. The resulting turquoise precipitate was collected, washed with water and ethanol, and dried in vacuo. Mass: 109 mg (0.14 mmol, 43%). Accurate Mass MS: Calculated for $C_{26}H_{44}O_2RuS_4$ [M^+ - PF_6]: 618.1268. Found: 618.1274 ± 1.0 PPM. Elemental Analysis: $C_{26}H_{44}F_6O_2PRuS_4$: calcd. C, 40.93; H, 5.81; found C = 40.97%, H = 5.50%.

7. [Ru([12]aneS_4)(DMSO)Cl](PF_6) (200 mg, 0.33 mmol) and $AgNO_3$ (57 mg, 0.33 mmol) were refluxed in 20 cm^3 of ethanol/water 1:1 for 1 h. After removal of precipitated AgCl by filtration, tetrachlorocatechol (100 mg, 1.5 equivalents) was added along with 1,2,2,6,6-pentamethylpiperidine (0.5 cm^3, excess), and the mixture brought to reflux, at which time an orange precipitate began to appear. The mixture was refluxed for 2 h, by which time a large amount of precipitate had formed. Upon cooling, the orange solid was collected by filtration, washed with water and ethanol and dried in vacuo Mass: 156 mg (0.27 mmol, 81%). ^{1}H NMR (d_6-DMSO): δ_H = 3.0 (broad m). Accurate Mass MS: Calculated for $C_{14}H_{16}Cl_4O_2RuS_4$ [M^+]: 587.4176. Found: 587.4155 ± 4.8 PPM. Elemental Analysis: $C_{14}H_{16}Cl_4O_2RuS_4$: calcd. C, 28.63; H, 2.75; found C = 28.77%, H = 2.49%.

8. This was synthesized using the same procedure as **7**, but with the following differences: [Ru([14]aneS_4)(DMSO)Cl](PF_6) (209 mg, 0.33 mmol), $AgNO_3$ (57 mg, 0.33 mmol), and 100 mg of tetrachlorocatechol were used. Upon cooling, the lime green solid was collected by filtration, washed with water and ethanol, and dried in vacuo Mass: 162 mg (0.26 mmol, 80%). ^{1}H NMR (d_6-DMSO): δ_H = 3.0 (m, 16H); 1.9 (m, 4H). Accurate Mass MS: Calculated for $C_{16}H_{20}Cl_4O_2RuS_4$ [M^+]: 613.8144. Found: 613.8212 ± 1.0 PPM. Elemental Analysis (for [**8**]·H_2O): $C_{16}H_{22}Cl_4O_3RuS_4$: calcd. C, 30.34; H, 3.50; found C = 30.34%, H = 3.66%.

9. This was synthesized using the same procedure as **7**, but with the following differences: [Ru([16]aneS_4)(DMSO)Cl](PF_6) (150 mg, 0.23 mmol), $AgNO_3$ (39 mg, 0.23 mmol), and 70 mg of tetrachlorocatechol were used. Upon cooling, the bright orange solid was collected by filtration, washed with water and ethanol, and dried in vacuo. Mass: 129 mg (0.20 mmol, 87%). ^{1}H NMR (d_6-DMSO): δ_H = 3.0 (broad m). Accurate Mass MS: Calculated for $C_{18}H_{24}Cl_4O_2RuS_4$ [M^+]: 641.8457. Found: 641.8444 ± 1.5 PPM. Elemental Analysis: $C_{18}H_{24}Cl_4O_2RuS_4$: calcd. C, 33.60; H, 3. 76; found C = 33.95%, H = 4.13%.

Crystallographic Determination. Crystals of [**8**]·H_2O were grown by "reverse vapor diffusion" from dichloromethane and hexane solutions. Relevant crystallographic data are summarized in Table 6. Data were collected at 100 K on a Bruker Smart CCD area detector with Oxford Cryosystems low temperature system and complex scattering factors were taken from the program package SHELXTL.[35]

Table 6. Crystal Data and Selected Structure Refinement Details for 8·H_2O

empirical formula	$C_{16}H_{22}Cl_4O_3RuS_4$
M	633.45
crystal system	triclinic
space group	$P\bar{1}$
crystal dimensions/mm	0.21 × 0.10 × 0.10
a /Å	9.2289(1)
b /Å	11.2430(1)
c /Å	12.3239(1)
α /deg	78.690(1)
β /deg	70.363(1)
γ /deg	67.037(1)
U /Å^3	1105.807(18)
Z	2
D_c /Mg/m^3	1.902
μ(Mo−Kα)/mm^{-1}	1.587
R_1, wR_2 [$I > 2\sigma I$]	0.0200, 0.0439
R_1, wR_2 (all data)	0.0230, 0.0451

The macrocycle was refined in two alternative positions with occupancies of 0.667(6) and 0.333(6) respectively. Anisotropic thermal parameters were used for all non-hydrogen atoms. Hydrogen atoms were placed geometrically and refined with a riding model and with U_{iso} constrained to be 1.2 times U_{eq} of the carrier atom. Molecular diagrams were drawn with PLATON[36] and ORTEP-3.[37]

DFT Calculations. All DFT calculations were performed with the Gaussian09 package[38] with the B3LYP functional.[28] A standard 6-311G(d) basis set[30] was used for all elements except for sulfur, where the aug-cc-pVQZ basis set,[32] was employed. The ruthenium was described using the recently developed LANL2TZ(f) basis set[29] with the associated ECP. This is a triple ξ basis set and includes an f polarization function. Spin unrestricted calculations were performed for the paramagnetic species, and the geometry optimizations were performed without constraints with acetonitrile as solvent using a polarizable continuum model described with the integral equation formalism variant (IEFPCM) as implemented in Gausian09.[39] The TD-DFT calculations were also performed using the Gaussian09 implementation on the B3LYP-optimized structures. The treatment of the TD-DFT data, including the scripts to plot the Electron Density Difference Maps upon electronic excitation, was performed with the GaussSum package.[40]

■ ASSOCIATED CONTENT

Supporting Information

X-ray crystallographic data for [8]·H_2O in CIF format. Histogram for the distribution of the ξ angles on Ru-TCC complexes, cyclic voltammograms for the reversible redox couples of the complexes **7** and **8**, figures and tables with DFT optimized structural parameters and molecular orbital compositions. The Cartesian coordinates of all optimized complexes. This material is available free of charge via the Internet at http://pubs.acs.org.

■ AUTHOR INFORMATION

Corresponding Author

*E-mail: m.d.ward@sheffield.ac.uk (M.D.W.), vitor.felix@ua.pt (V.F.), james.thomas@sheffield.ac.uk (J.A.T.).

Notes

The authors declare no competing financial interest.

■ ACKNOWLEDGMENTS

P.J.C. thanks FCT for a postdoctoral grant (SFRH/BPD/27082/2006). We also thank to "Anglo-Portuguese Joint Research Programme-Treaty of Windsor" for travel grants.

■ REFERENCES

(1) (a) Jørgensen, C. K. *Coord. Chem. Rev.* **1966**, *1*, 164. (b) Stiefel, E. I.; Eisenberg, R.; Rosenberg, R. C.; Gray, H. B. *J. Am. Chem. Soc.* **1966**, *88*, 2956. (c) McCleverty, J. A. *Prog. Inorg. Chem.* **1968**, *10*, 49. (d) Ward, M. D.; McCleverty, J. A. *Dalton Trans.* **2002**, 275. (e) Ray, K.; Petrenko, T.; Wieghardt, K.; Neese, F. *Dalton Trans.* **2007**, 1552. (f) Sproules, S.; Wieghardt, K. *Coord. Chem. Rev.* **2010**, *254*, 1358. (g) Lever, A. P. B. *Coord. Chem. Rev.* **2010**, *254*, 1394.

(2) (a) Stubbe, J.; van der Donk, W. A. *Chem. Rev.* **1998**, *98*, 705. (b) Jazdzewski, B. A.; Tolman, W. B. *Coord. Chem. Rev.* **2000**, *200*−*202*, 633. (c) Chaudhuri, P.; Wieghardt, K. *Prog. Inorg. Chem.* **2001**, *50*, 151.

(3) (a) Zarkesh, R. A.; Ziller, J. W.; Heyduk, A. F. *Angew. Chem., Int. Ed.* **2008**, *47*, 4715. (b) Chirik, P. J.; Wieghardt, K. *Science* **2010**, *327*, 794. (c) Boyer, J. L.; Rochford, J.; Tsai, M.-K.; Muckerman, J. T.; Fujita, E. *Coord. Chem. Rev.* **2010**, *254*, 309.

(4) (a) Gray, H. B.; Williams, R.; Bernal, I.; Billig, E. *J. Am. Chem. Soc.* **1962**, *84*, 3596. (b) Davison, A.; Edelstein, N.; Holm, R. H.; Maki, A. H. *J. Am. Chem. Soc.* **1963**, *85*, 2029. (c) Eisenberg, R. *Coord. Chem. Rev.* **2011**, *255*, 825.

(5) (a) Pierpont, C. G.; Downs, H. H.; Rukavina, T. G. *J. Am. Chem. Soc.* **1974**, *96*, 5573. (b) Pierpont, C. G.; Lange, C. W. *Prog. Inorg. Chem.* **1994**, *41*, 331.

(6) Sofen, S. R.; Ware, D. C.; Cooper, S. R.; Raymond, K. N. *Inorg. Chem.* **1979**, *18*, 234.

(7) Balch, A. L.; Sohn, Y. S. *J. Organomet. Chem.* **1971**, *30*, C31.

(8) Haga, M.; Dodsworth, E. S.; Lever, A. B. P. *Inorg. Chem.* **1986**, *25*, 447.

(9) Masui, H.; Auburn, P. R.; Lever, A. B. P. *Inorg. Chem.* **1991**, *30*, 2402−2410.

(10) Ebadi, M.; Lever, A. B. P. *Inorg. Chem.* **1999**, *38*, 467.

(11) Lever, A. B. P.; Masui, H.; Metcalfe, R. A.; Stufkens, D. J.; Dodsworth, E. S.; Auburn, P. R. *Coord. Chem. Rev.* **1993**, *125*, 317.

(12) Gorelsky, S. I.; Dodsworth, E. S.; Lever, A. B. P.; Vlcek, A. A. *Coord. Chem. Rev.* **1998**, *174*, 469.

(13) See for example: (a) Joulié, L. F.; Schatz, E.; Ward, M. D.; Weber, F.; Yellowlees, L. J. *Dalton Trans.* **1994**, 799. (b) Barthram, A. M.; Cleary, R. L.; Kowallick, R.; Ward, M. D. *Chem. Commun.* **1998**, 2695.

(14) Grange, C. S.; Meijer, A. J. H. M.; Ward, M. D. *Dalton Trans.* **2010**, *39*, 200.

(15) (a) García-Cañadas, J.; Meacham, A. P.; Peter, L. M.; Ward, M. D. *Angew. Chem., Int. Ed.* **2003**, *42*, 3011. (b) Vickers, S. J.; Ward, M. D. *Electrochem. Commun.* **2005**, *7*, 389.

(16) (a) Goodfellow, B. J.; Pacheco, S. M. D.; Pedrosa de Jesus, J. P.; Felix, V.; Drew, M. G. B. *Polyhedron* **1997**, *16*, 3293. (b) Santos, T. M.; Goodfellow, B. J.; Madureira, J.; Pedrosa de Jesus, J.; Félix, V.; Drew, M. G. B. *New J. Chem.* **1999**, *23*, 1015.

(17) Adams, H.; Amado, A. M.; Félix, V.; Mann, B. E.; Antelo-Martinez, J.; Newell, M.; Ribeiro-Claro, P. J. A.; Spey, S. E.; Thomas, J. A. *Chem.—Eur. J.* **2005**, *11*, 2031.

(18) Roche, S.; Yellowlees, L. J.; Thomas, J. A. *Chem. Commun.* **1998**, 1429.

(19) Araújo, C. S.; Drew, M. G. B.; Félix, V.; Jack, L.; Madureira, J.; Newell, M.; Roche, S.; Santos, T. M.; Thomas, J. A.; Yellowlees, L. J. *Inorg. Chem.* **2002**, *41*, 2260.

(20) Newell, M.; Thomas, J. A. *Dalton Trans.* **2006**, 705.

(21) Newell, M.; Ingram, J. D.; Easun, T. L.; Vickers, S.; Adams, H.; Ward, M. D.; Thomas, J. A. *Inorg. Chem.* **2006**, *45*, 821.

(22) Adams, H.; Costa, P. J.; Newell, M.; Vickers, S. J.; Ward, M. D.; Félix, V.; Thomas, J. A. *Inorg. Chem.* **2008**, *47*, 11633.

(23) (a) Mullen, G. E. D.; Went, M. J.; Wocaldo, S.; Powell, A. K.; Blower, P. J. *Angew. Chem., Int. Ed. Engl.* **1997**, *36*, 1205. (b) Mullen,

G. E. D.; Fässler, T. F.; Went, M. J.; Howland, K.; Stein, B.; Blower, P. J. *J. Chem. Soc., Dalton Trans.* **1999**, 3759.
(24) Shan, N.; Vickers, S.; Adams, H.; Ward, M. D.; Thomas, J. A. *Angew. Chem., Int. Ed.* **2004**, *43*, 3938.
(25) Shan, N.; Ingram, J. D.; Easun, T. L.; Vickers, S.; Adams, H.; Ward, M. D.; Thomas, J. A. *Dalton Trans* **2006**, 2900.
(26) Brandt, K.; Shedrick, W. S. *J. Chem. Soc., Dalton Trans.* **1996**, 1237.
(27) Allen, F. H. *Acta Crystallogr.* **2002**, *B58*, 380.
(28) (a) Becke, A. D. J. *Chem. Phys.* **1993**, *98*, 5648. (b) Lee, C.; Yang, W.; Parr, R. G. *Phys. Rev. B* **1988**, *37*, 785.
(29) Roy, L. E.; Hay, P. J.; Martin, R. L. *J. Chem. Theory Comput.* **2008**, *4*, 1029.
(30) Krishnan, R.; Binkley, J. S.; Seeger, R.; Pople, J. A. *J. Chem. Phys.* **1980**, *72*, 650.
(31) One referee pointed out that this discrepancy might be due to the use of an inappropriate basis set for sulfur (6-311G*) in reference 22. However, all tested basis sets give longer bonds.
(32) Woon, D. E.; Dunning, T. H., Jr. *J. Chem. Phys.* **1993**, *98*, 1358.
(33) Casida, M. E.; Ipatov, A.; Cordova, F. *Lect. Notes Phys.* **2006**, *706*, 243−257.
(34) Ipatov, A.; Cordova, F.; Doriol, L. J.; Casida, M. E. *J. Mol. Struc.:THEOCHEM* **2009**, *914*, 60−73.
(35) Sheldrick, G. M. *Acta Crystallogr.* **2008**, *A64*, 112.
(36) Spek, A. L. *Acta Crystallogr.* **2009**, *D65*, 148.
(37) Farrugia, L. J. *J. Appl. Crystallogr.* **1997**, *30*, 565.
(38) Frisch, M. J.; Trucks, G. W.; Schlegel, H. B.; Scuseria, G. E.; Robb, M. A.; Cheeseman, J. R.; Zakrzewski, V. G.; Montgomery, Jr., J. A.; Stratmann, R. E.; Burant, J. C.; Dapprich, S.; Millam, J. M.; Daniels, A. D.; Kudin, K. N.; Strain, M. C.; Farkas, O.; Tomasi, J.; Barone, V.; Cossi, M.; Cammi, R.; Mennucci, B.; Pomelli, C.; Adamo, C.; Clifford, S.; Ochterski, J.; Petersson, G. A.; Ayala, P. Y.; Cui, Q.; Morokuma, K.; Rega, N.; Salvador, P.; Dannenberg, J. J.; Malick, D. K.; Rabuck, A. D.; Raghavachari, K.; Foresman, J. B.; Cioslowski, J.; Ortiz, J. V.; Baboul, A. G.; Stefanov, B. B.; Liu, G.; Liashenko, A.; Piskorz, P.; Komaromi, I.; Gomperts, R.; Martin, R. L.; Fox, D. J.; Keith, T.; Al-Laham, M. A.; Peng, C. Y.; Nanayakkara, A.; Challacombe, M.; Gill, P. M. W.; Johnson, B.; Chen, W.; Wong, M. W.; Andres, J. L.; Gonzalez, C.; Head-Gordon, M.; Replogle, E. S.; Pople, J. A. *Gaussian 09*, Revision A.01; Gaussian, Inc.: Wallingford, CT, 2009.
(39) Barone, V.; Cossi, M.; Tomasi, J. *J. Chem. Phys.* **2002**, *107*, 43−54.
(40) O'Boyle, N. M.; Tenderholt, A. L.; Langner, K. M. *J. Comput. Chem.* **2008**, *29*, 839.